Available online at www.sciencedirect.com
ScienceDirect
Journal of Sound and Vibration 304 (2007) 326–344
JOURNAL OF SOUND AND VIBRATION
www.elsevier.com/locate/jsvi

Parametric instability regions of three-layered soft-cored sandwich beam using higher-order theory

S.K. Dwivedy*, K.C. Sahu, Sk. Babu

Mechanical Engineering Department, Indian Institute of Technology, Guwahati 781 039, India

Received 2 February 2006; received in revised form 29 August 2006; accepted 3 March 2007

Abstract

The purpose of the present work is to study the parametric instability of a three-layered, soft-cored, symmetric sandwich beam subjected to a periodic axial load. Due to soft core, the displacements of the top and bottom skins are different and hence, instead of using the classical theory a higher-order theory is used. Using extended Hamilton's principle and taking beam theory for the skins and a two-dimensional theory for the core, the governing equations of motion and boundary conditions are derived. A generalized Galerkin's method is used to reduce the equations of motion to a set of non-dimensional coupled Mathieu–Hill's equations with complex coefficients. The parametric instability regions for simple and combination resonances are investigated for simply supported, clamped–guided, clamped–free riveted and clamped–free end conditions by modified Hsu's method. The influences of shear parameter; the core loss-factor and the ratio of core thickness to skin thickness on the zones of instability have been studied. This general analysis can be applied to sandwich beams with a flexible core and any type of construction. The results are compared with those reported for classical theories.

1. Introduction

To suppress vibration and noise in machines, automobiles, aircrafts, home appliances, etc. one may use viscoelastic materials sandwiched between elastic layers. In these arrangements, energy is dissipated due to cyclic deformation of the viscoelastic materials, which results in damping the vibration. Mainly the use of multilayered structures with suitable arrangements of elastic and viscoelastic layers is gaining importance in damping the vibrations of structures subjected to a wide range of excitation frequencies.

Most of the studies of sandwich structure [1–7] are devoted to the free vibration analysis without considering the core to be flexible in transverse direction. In these cases, the governing equations of motion of the sandwich structure are developed based on the classical principle or the anti-plane concept which implies that the deflections of the upper and lower faces are equal and the longitudinal displacement distribution throughout the height of the core is linear. The classical theory is no longer valid when one uses foam-like core material [8] and hence a higher-order theory, which takes both the nonlinear displacement fields of the core material and realistic supports into account should be used. Frostig and Baruch [9], Frostig [10], Bremen et al.

*Corresponding author. Fax: +91 361 269 0762.
E-mail address: dwivedy@iitg.ernet.in (S.K. Dwivedy).

0022-460X/$ - see front matter © 2007 Elsevier Ltd. All rights reserved.
doi:10.1016/j.jsv.2007.03.016

[11], Sokolinsky et al. [12], Sokolinsky and Nutt [13], Frostig and Thomsen [14], Yang and Qiao [15] and Liu and Zhao [16] studied sandwich beams with soft core using higher-order theory. In all these cases the study is limited to free vibration analysis of the systems. One may refer Noor et al. [17], Sun and Lu [18] and David [19] for a comprehensive knowledge of modeling, damping properties and applications of sandwich structures.

In many applications these sandwich structures are subjected to parametric excitation. Unlike the forced vibration in which the resonance occurs only when the excitation frequency is equal to one of the modal frequencies, in case of parametric excitation, a small excitation can produce a large response when the frequency of the excitation is close to twice the natural frequencies (*principal parametric resonance)* or combination of different modal frequencies (*combination resonances*). A general description of the parametrically excited system can be obtained in the texts by Nayfeh and Mook [20], Cartmell [21]. Some of the literature considering parametric excitation on sandwich beam/columns includes those of Bauld [22], Saito and Otomi [23], Chonan [24], Kar and Sujata [25], Ray and Kar [26,27]. In all these cases the dynamic stability of sandwich structures have been studied and the parametric instability regions are plotted for different system parameters. Saito and Otomi [23] modified Hsu [28] procedure to determine the stability of viscoelastic beams with an attached mass and viscoelastic end supports under axial and tangential periodic loads. Kar and Sujata [25] and Ray and Kar [26,27] obtained the parametric instability regions for simple and combination resonances for different types of sandwich beams with viscoelastic core using the modified Hsu procedure.

In all the above-mentioned works on parametric instability of sandwich beam, the core was not considered to be flexible in the transverse direction and hence the anti-plane concept were used to model the sandwich structure. To the best of the authors' knowledge no work has been reported to study the stability of soft core (which are flexible in transverse direction) sandwich beam subjected to parametric excitation. So in this work an effort has been made to develop the governing equation of motion of such systems using higher-order theory [9,10] and Hamilton's principle, and then to obtain the parametric instability regions for different system parameters. This study will be very much useful to the researcher/designer to suppress vibration using soft-cored sandwich structures.

2. Formulation of the problem

Fig. 1 shows a simply supported, symmetric, three-layered sandwich beam of length L and width b with a flexible soft core. The top, core and bottom layer thickness are d_t, c and d_b, respectively. The upper and lower layers (face layer) of the beam are of the same elastic material and the core is of soft viscoelastic material. The sandwich beam is subjected to an axial periodic load $P(t) = P_0 + P_1 \cos \omega t$, ω being the frequency of the applied load, t being the time and P_0 and P_1 are the amplitudes of static and dynamic load, respectively.

Fig. 2 shows the geometry of the sandwich beam, the load and internal forces and moments in different layers and the deflection in x and z directions before and after deformations. Here, Q_{xx} is the shear force, N_{xx} is the axial force and M_{xx} is the bending moment. Superscripts t and b represent the top and bottom layer, respectively. The assumptions made for deriving the governing equations are similar to that by Frostig [10] and are (i) the face sheets of the sandwich beam are modeled as Euler–Bernoulli beams (ii) the transversely

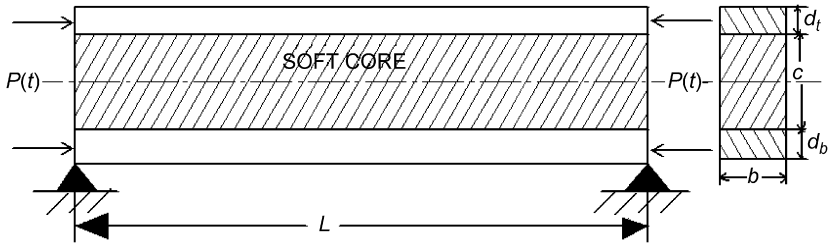

Fig. 1. Symmetric three-layered sandwich beam with soft core.

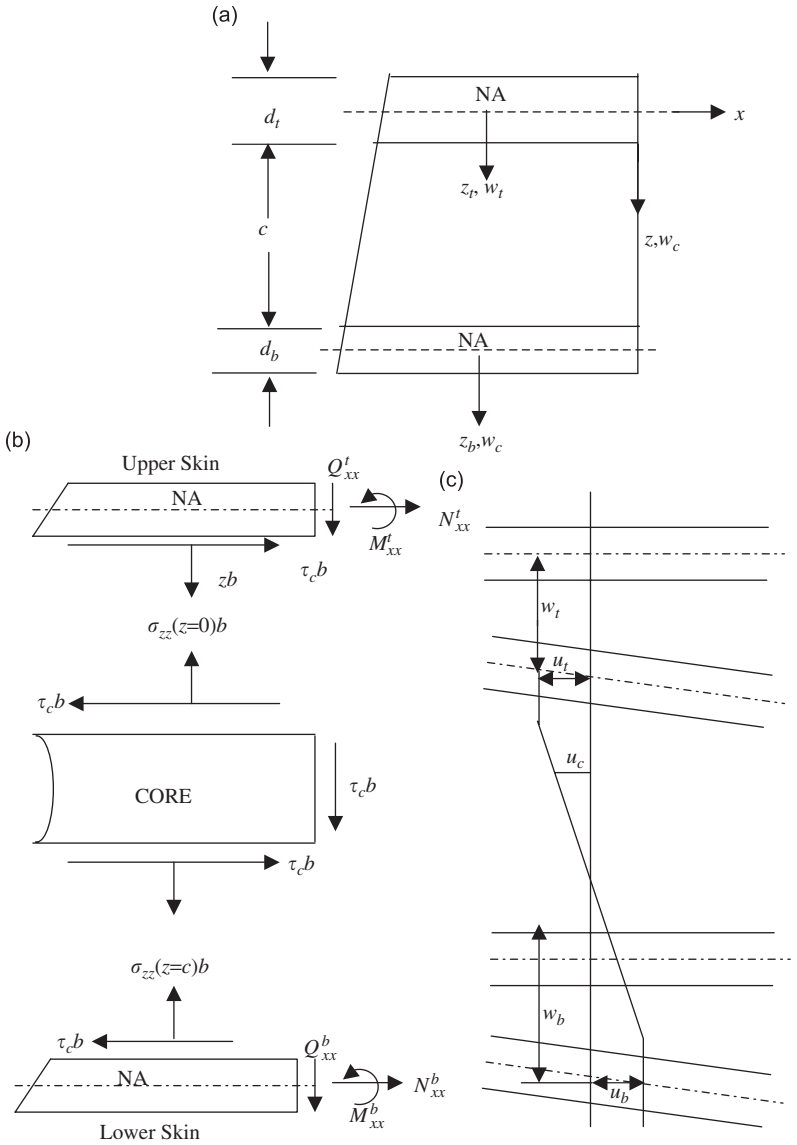

Fig. 2. (a) Geometry, (b) load, internal forces and moments (c) displacement pattern through depth of section. N.A is the neutral axis.

flexible core layer is considered as a two-dimensional elastic medium with small deformations where its height may change under loading, and its cross-section does not remain planar. The longitudinal (in-plane) stresses in the core are neglected and (iii) the interface layers between the face sheets and the core are assumed to be infinitely rigid and provide perfect continuity of the deformations at the interfaces.

The internal potential energy (U) in terms of direct stresses (σ) and shear stress τ and strains (ε, γ) is given by

$$U = \int_{v_{\text{top}}} \sigma_{xx}\varepsilon_{xx}\,\mathrm{d}v + \int_{v_{\text{bot}}} \sigma_{xx}\varepsilon_{xx}\,\mathrm{d}v + \int_{v_{\text{core}}} \tau_c\gamma_c\,\mathrm{d}v + \int_{v_{\text{core}}} \sigma_{zz}\varepsilon_{zz}\,\mathrm{d}v, \tag{1}$$

where v_{top}, v_{bot}, and v_{core} are the volume of the top, bottom and core layer, respectively. One may note that, as the core is taken to be flexible, deformation takes place in the transverse direction (z direction) and the last

term of Eq. (1) takes care of that effect. The kinetic energy T can be given by

$$T = (1/2)\left\{\int_0^L m_t(\dot{u}_t^2 + \dot{w}_t^2)\,\mathrm{d}x + \int_0^L m_b(\dot{u}_b^2 + \dot{w}_b^2)\,\mathrm{d}x + \int_{v_{\text{core}}} \rho_c \dot{u}_c^2\,\mathrm{d}v + \int_{v_{\text{core}}} \rho_c \dot{w}_c^2\,\mathrm{d}v\right\}. \tag{2}$$

Here m_t and m_b are the mass per unit length of the top and bottom layer, respectively, and ρ_c is the density of the core material; u_t and u_b are the displacement at the neutral axis of the top and bottom layer along x (longitudinal) direction, respectively; w_t and w_b are the displacement at top and bottom layer along z (vertical) direction, respectively (Fig. 2(c)). Also, u_c and w_c are the displacement of the core along x and z directions, respectively, and can be given by [9]

$$u_c = u_t - (d_t/2)w_{t,x} + \frac{\{u_b + (d_b/2)w_{b,x} - (u_t - (d_t/2)w_{t,x})\}z}{c}, \tag{3a}$$

$$w_c = w_t + \frac{(w_b - w_t)z}{c}. \tag{3b}$$

Here $()_{,x}$ represents the differentiation with respect to x and subscripts t, b, c represent top, bottom and core layer, respectively.

The non-conservative work done due to the applied load can be given by

$$W_{nc} = (1/2)\left(\int_0^L P w_{t,x}^2 \mathrm{d}x + \int_0^L P w_{b,x}^2 \mathrm{d}x\right). \tag{4}$$

The following non-dimensional parameters are used in this analysis

$$\begin{aligned}
&\bar{P}_0 = P_0 L^2/(2E_q I_q), \quad \bar{P}_1 = P_1 L^2/(2E_q I_q), \quad \xi_c = G_c^* A_c L^2/E, \quad \phi_t = E_t A_t L^2/E, \quad \phi_b = E_b A_b L^2/E,\\
&\phi_c = E_c A_c L^2/E, \quad g = G_c/(E_t(c/d_t)(L/d_t)^2 + E_b(c/d_b)(L/d_b)^2), \quad \bar{t} = t/t_0, \quad \bar{x} = x/L,\\
&\bar{u}_q = u_q/L, \quad \bar{w}_q = w_q/L, \quad \bar{m}_q = m_q/m, \quad \bar{m}_c = m_c/m.
\end{aligned} \tag{5}$$

Here, $\bar{P}_0$ and $\bar{P}_1$ are, respectively, the non-dimensional static and dynamic load amplitudes; E_q, I_q and A_q are the Young's modulus, moment of inertia and the area of cross-section of the qth layer (q equal to t for top layer and b for bottom layer); $E = E_t I_t + E_b I_b$; E_c, A_c and m_c are the Young's modulus, area of cross-section and mass per unit length of the core, respectively. The non-dimensional time, $t_0 = (mL^4/E)^{(1/2)}$, where m is the total mass per unit length. The complex shear modulus of the viscoelastic core is given by $G_c^* = G_c(1 + \mathrm{j}\eta_c)$, where G_c is the phase shear modulus, $\mathrm{j} = \sqrt{-1}$ and η_c is the core loss factor. The non-dimensional term g is known as the shear parameter of the system.

Using Eqs. (1)–(5), the governing non-dimensional equations of motion and the boundary conditions are derived by applying the extended Hamilton's principle. These resulting governing equations of motion are as follows:

$$\begin{aligned}
&(\bar{m}_t + \bar{m}_c/3)\ddot{\bar{w}}_t - (\bar{m}_c/12)(d_t/c)^2(c/L)^2\ddot{\bar{w}}_{t,\bar{x}\bar{x}} + (\bar{m}_c/576)(d_t/c)\{1 + (d_t/c)\}(c/L)^4(\xi_c/\phi_c)\ddot{\bar{w}}_{t,\bar{x}\bar{x}\bar{x}\bar{x}}\\
&\quad + (\bar{m}_c/24)(d_t/c)(d_b/c)(c/L)^2\ddot{\bar{w}}_{b,\bar{x}\bar{x}} + (\bar{m}_c/576)(d_b/c)\{1 + (d_t/c)\}(c/L)^4(\xi_c/\phi_c)\ddot{\bar{w}}_{b,\bar{x}\bar{x}\bar{x}\bar{x}}\\
&\quad + (\bar{m}_c/6)\ddot{\bar{w}}_b + (\bar{m}_c/6)(d_t/c)(c/L)\ddot{\bar{u}}_{t,\bar{x}} - (1/48)(\bar{m}_t + \bar{m}_c/6)\{1 + (d_t/c)\}(c/L)^3(\xi_c/\phi_c)\ddot{\bar{u}}_{t,\bar{x}\bar{x}\bar{x}}\\
&\quad + (\bar{m}_c/12)(d_t/c)(c/L)\ddot{\bar{u}}_{b,\bar{x}} + (1/48)(\bar{m}_b + \bar{m}_c/6)\{1 + (d_t/c)\}(c/L)^3(\xi_c/\phi_c)\ddot{\bar{u}}_{b,\bar{x}\bar{x}\bar{x}}\\
&\quad - \phi_c(L/c)^2\bar{w}_t - (\xi_c/4)\{1 + (d_t/c)\}^2\bar{w}_{t,\bar{x}\bar{x}} - \phi_c(L/c)^2\bar{w}_b - (\xi_c/4)\{1 + (d_t/c)\}\{1 + (d_b/c)\}\bar{w}_{b,\bar{x}\bar{x}}\\
&\quad + (\xi_c/2)(L/c)\{1 + (d_t/c)\}\bar{u}_{t,\bar{x}} + (\xi_c/\phi_c)\{1 + (d_t/c)\}(\phi_t/48)(c/L)^3\bar{u}_{t,\bar{x}\bar{x}\bar{x}\bar{x}\bar{x}}\\
&\quad - (\xi_c/2)(L/c)\{1 + (d_t/c)\}\bar{u}_{b,\bar{x}} - (\xi_c/\phi_c)\{1 + (d_t/c)\}(\phi_b/48)(c/L)^3\bar{u}_{b,\bar{x}\bar{x}\bar{x}\bar{x}\bar{x}}\\
&\quad + (\phi_t/12)(d_t/c)^2(c/L)^2\bar{w}_{t,\bar{x}\bar{x}\bar{x}\bar{x}} + (PL^2/E)\bar{w}_{t,\bar{x}\bar{x}} = 0,
\end{aligned} \tag{6}$$

$$
\begin{aligned}
&(\bar{m}_c/6)\ddot{\bar{w}}_t + (\bar{m}_c/24)(d_t/c)(d_b/c)(c/L)^2\ddot{\bar{w}}_{t,\bar{x}\bar{x}} + (\bar{m}_c/576)(d_t/c)\{1+(d_b/c)\}(c/L)^4(\xi_c/\phi_c)\ddot{\bar{w}}_{t,\bar{x}\bar{x}\bar{x}\bar{x}}\\
&\quad + (\bar{m}_b + \bar{m}_c/3)\ddot{\bar{w}}_b - (\bar{m}_c/12)(d_t/c)^2(c/L)^2\ddot{\bar{w}}_{b,\bar{x}\bar{x}} + (\bar{m}_c/576)(d_b/c)\{1+(d_b/c)\}(c/L)^4(\xi_c/\phi_c)\ddot{\bar{w}}_{b,\bar{x}\bar{x}\bar{x}\bar{x}}\\
&\quad - (\bar{m}_c/12)(d_b/c)(c/L)\ddot{\bar{u}}_{t,\bar{x}} - (1/48)(\bar{m}_t + \bar{m}_c/6)\{1+(d_b/c)\}(c/L)^3(\xi_c/\phi_c)\ddot{\bar{u}}_{t,\bar{x}\bar{x}\bar{x}} - (\bar{m}_c/6)(d_b/c)(c/L)\ddot{\bar{u}}_{b,\bar{x}}\\
&\quad + (1/48)(\bar{m}_b + \bar{m}_c/6)\{1+(d_b/c)\}(c/L)^3(\xi_c/\phi_c)\ddot{\bar{u}}_{b,\bar{x}\bar{x}\bar{x}} + \phi_c(L/c)^2\bar{w}_b - (\xi_c/4)\{1+(d_t/c)\}\{1+(d_b/c)\}\bar{w}_{t,\bar{x}\bar{x}}\\
&\quad - \phi_c(L/c)^2\bar{w}_t - (\xi_c/4)\{1+(d_b/c)\}^2\bar{w}_{b,\bar{x}\bar{x}} + (\xi_c/2)(L/c)\{1+(d_b/c)\}\bar{u}_{t,\bar{x}}\\
&\quad + (\xi_c/\phi_c)\{1+(d_b/c)\}(\phi_t/48)(c/L)^3\bar{u}_{t,\bar{x}\bar{x}\bar{x}\bar{x}\bar{x}} - (\xi_c/2)(L/c)\{1+(d_b/c)\}\bar{u}_{b,\bar{x}}\\
&\quad - (\xi_c/\phi_c)\{1+(d_b/c)\}(\phi_b/48)(c/L)^3\bar{u}_{b,\bar{x}\bar{x}\bar{x}\bar{x}\bar{x}} + (\phi_b/12)(d_b/c)^2(c/L)^2\bar{w}_{b,\bar{x}\bar{x}\bar{x}\bar{x}} + (PL^2/E)\bar{w}_{b,\bar{x}\bar{x}} = 0,
\end{aligned}
\tag{7}
$$

$$
\begin{aligned}
&(\bar{m}_c/6)(d_t/c)(c/L)\ddot{\bar{w}}_{t,\bar{x}} - (\bar{m}_c/288)(d_t/c)(c/L)^3(\xi_c/\phi_c)\ddot{\bar{w}}_{t,\bar{x}\bar{x}\bar{x}}\\
&\quad - (\bar{m}_c/12)(d_b/c)(c/L)\ddot{\bar{w}}_{b,\bar{x}} - (\bar{m}_c/288)(d_b/c)(c/L)^3(\xi_c/\phi_c)\ddot{\bar{w}}_{b,\bar{x}\bar{x}\bar{x}}\\
&\quad + (1/24)(\bar{m}_t + \bar{m}_c/6)(c/L)^2(\xi_c/\phi_c)\ddot{\bar{u}}_{t,\bar{x}\bar{x}} - (\bar{m}_t + \bar{m}_c/3)\ddot{\bar{u}}_t\\
&\quad - (1/24)(\bar{m}_b + \bar{m}_c/6)(c/L)^2(\xi_c/\phi_c)\ddot{\bar{u}}_{b,\bar{x}\bar{x}} - (\bar{m}_c/6)\ddot{\bar{u}}_b + (\xi_c/2)\{1+(d_t/c)\}(L/c)\bar{w}_{t,\bar{x}}\\
&\quad + (\xi_c/2)(L/c)\{1+(d_b/c)\}\bar{w}_{b,\bar{x}} + \phi_t\bar{u}_{t,\bar{x}\bar{x}} - (L/c)^2\xi_c\bar{u}_t - (\xi_c/\phi_c)(\phi_t/24)(c/L)^2\bar{u}_{t,\bar{x}\bar{x}\bar{x}\bar{x}}\\
&\quad + (L/c)^2\xi_c\bar{u}_b + (\xi_c/\phi_c)(\phi_b/24)(c/L)^2\bar{u}_{b,\bar{x}\bar{x}\bar{x}\bar{x}} = 0,
\end{aligned}
\tag{8}
$$

$$
\begin{aligned}
&(\bar{m}_c/12)(d_t/c)(c/L)\ddot{\bar{w}}_{t,\bar{x}} + (\bar{m}_c/288)(d_t/c)(c/L)^3(\xi_c/\phi_c)\ddot{\bar{w}}_{t,\bar{x}\bar{x}\bar{x}}\\
&\quad - (\bar{m}_c/6)(d_b/c)(c/L)\ddot{\bar{w}}_{b,\bar{x}} + (\bar{m}_c/288)(d_b/c)(c/L)^3(\xi_c/\phi_c)\ddot{\bar{w}}_{b,\bar{x}\bar{x}\bar{x}}\\
&\quad - (\bar{m}_c/6)\ddot{\bar{u}}_t - (1/24)(\bar{m}_t + \bar{m}_c/6)(c/L)^2(\xi_c/\phi_c)\ddot{\bar{u}}_{t,\bar{x}\bar{x}} - (\bar{m}_b + \bar{m}_c/3)\ddot{\bar{u}}_b\\
&\quad + (1/24)(\bar{m}_b + \bar{m}_c/6)(c/L)^2(\xi_c/\phi_c)\ddot{\bar{u}}_{b,\bar{x}\bar{x}} - (\xi_c/2)\{1+(d_t/c)\}(L/c)\bar{w}_{t,\bar{x}}\\
&\quad - (\xi_c/2)(L/c)\{1+(d_b/c)\}\bar{w}_{b,\bar{x}} + (L/c)^2\xi_c\bar{u}_t + (\xi_c/\phi_c)(\phi_t/24)(c/L)^2\bar{u}_{t,\bar{x}\bar{x}\bar{x}\bar{x}}\\
&\quad + \phi_b\bar{u}_{b,\bar{x}\bar{x}} - (L/c)^2\xi_c\bar{u}_b - (\xi_c/\phi_c)(\phi_b/24)(c/L)^2\bar{u}_{b,\bar{x}\bar{x}\bar{x}\bar{x}} = 0.
\end{aligned}
\tag{9}
$$

3. Approximate solution

As the above equations of motion (6)–(9) are in space and time coordinates, generalized Galerkin's principle is used to reduce these equations to their temporal form. For multimode discretization one may take

$$
\bar{w}_t = \sum_{p=1}^{N} f_p(\bar{t})w_p(\bar{x}), \quad \bar{w}_b = \sum_{q=N+1}^{2N} f_q(\bar{t})w_q(\bar{x}), \quad \bar{u}_t = \sum_{r=2N+1}^{3N} f_r(\bar{t})u_r(\bar{x}), \quad \bar{u}_b = \sum_{s=3N+1}^{4N} f_s(\bar{t})u_s(\bar{x}). \tag{10}
$$

Here, N is a positive integer representing the number of modes taken in the analysis and $f_p(\bar{t})$, $f_q(\bar{t})$, $f_r(\bar{t})$, and $f_s(\bar{t})$ are the generalized coordinates and $w_p(\bar{x})$, $w_q(\bar{x})$, $u_r(\bar{x})$ and $u_s(\bar{x})$ are the shape functions chosen to satisfy as many as the boundary conditions. The resulting equation of motion becomes

$$
[M]\{\ddot{f}\} + [K]\{f\} - \bar{P}_1\cos\bar{\omega}\bar{t}[H]\{f\} = \{\phi\}. \tag{11}
$$

Here, $(\cdot) = \mathrm{d}(\,)/\mathrm{d}\bar{t}$, $\{f\} = \{\{f_p\}^{\mathrm{T}}\{f_q\}^{\mathrm{T}}\{f_r\}^{\mathrm{T}}\{f_s\}^{\mathrm{T}}\}^{\mathrm{T}}$, and $[K] = [K_1] - \bar{P}_0[H]$,

where

$$
[M] = \begin{bmatrix} [M_{11}] & [M_{12}] & [M_{13}] & [M_{14}] \\ [M_{21}] & [M_{22}] & [M_{23}] & [M_{24}] \\ [M_{31}] & [M_{32}] & [M_{33}] & [M_{34}] \\ [M_{41}] & [M_{42}] & [M_{43}] & [M_{44}] \end{bmatrix}, \quad [K_1] = \begin{bmatrix} [K_{11}] & [K_{12}] & [K_{13}] & [K_{14}] \\ [K_{21}] & [K_{22}] & [K_{23}] & [K_{24}] \\ [K_{31}] & [K_{32}] & [K_{33}] & [K_{34}] \\ [K_{41}] & [K_{42}] & [K_{43}] & [K_{44}] \end{bmatrix},
$$

$$[H]=\begin{bmatrix}[H_{11}] & [\phi] & [\phi] & [\phi]\\ [\phi] & [H_{22}] & [\phi] & [\phi]\\ [\phi] & [\phi] & [\phi] & [\phi]\\ [\phi] & [\phi] & [\phi] & [\phi]\end{bmatrix}, \quad \{\phi\} \text{ and } [\phi] \text{ are null matrices.}$$

The elements of the various sub matrices are given in the Appendix.

Eq. (11) is a set of coupled Mathieu–Hill equations with complex coefficients. In the absence of any external forcing, these equations reduce to those of Frostig and Baruch [9] where only the free-vibration study has been made. Also this equation is similar in form (but coefficients are different) to that obtained by Ray and Kar [26]. It may be noted that, Ray and Kar [26] have not considered the core to be flexible in transverse direction and hence used classical theory. For numerical calculations following shape functions are considered.

For simply supported beam

$$w_p(\bar{x})=\sin(p\pi\bar{x}), \quad w_q(\bar{x})=\sin(\bar{q}\pi\bar{x}), \quad u_r(\bar{x})=\cos(\bar{r}\pi\bar{x}) \text{ and } u_s(\bar{x})=\cos(\bar{s}\pi\bar{x}). \tag{12}$$

These shape functions satisfy all the boundary conditions. Here $p=1,2,\ldots,N$, $\bar{q}=(q-N)$, $\bar{r}=(r-2N)$ and $\bar{s}=(s-3N)$.

The following shape functions are used for clamped–guided beam [26].

$$\begin{aligned} w_i(\bar{x}) &= (i+3)(i+2)(i+1)\{2+(2-\mu_1)i\}\bar{x}^{(i+1)}-[2(i+3)(i+1)^2\{1+(2-\mu_1)i\}\\ &\quad+\mu_1\{(i+1)/\{2(i+2)+(2-\mu_1)(i+2)i\}\bar{x}^{(i+2)}\\ &\quad+[(i+2)(i+1)^2 i(2-\mu_1)-\mu_1 i(i+1)/\{2(i+3)+(2-\mu_1)(i+3)i\}]\bar{x}^{(i+3)}, \end{aligned} \tag{13a}$$

$$u_{\bar{k}}(\bar{x})=(\bar{k}+1)\bar{x}^{\bar{k}}-[2(\bar{k}+3)(\bar{k}+2)(\bar{k}+1)+\bar{k}\{1+\mu_1/(2+2\bar{k}-\mu_1\bar{k})\}]\bar{x}^{(\bar{k}+1)}, \tag{13b}$$

where $i=p$ for top layer and equal to $q-N$ for bottom layer and $\bar{k}$ equal to $r-2N$ for top layer and $s-3N$ for bottom layer. $\mu_1=Y/(1+Y)$ where, $Y=3(1+(c/d_t)^2)$, and $\mu_2=\bar{P}_0/(1+Y)$.

For clamped–free riveted beam, the shape functions can be given by [26]

$$\begin{aligned} w_i(\bar{x}) &= (i+3)(i+2)\{(i+2)(i+1)-\mu_2\}\bar{x}^{(i+1)}+[2(i+3)(i+1)\{\mu_2-i(i+2)\}\\ &\quad+\mu_1\{(i-1)(i+2)-\mu_2\}/\{(i+2)^2(i+1)-\mu_2(i+2)\}]\bar{x}^{(i+2)}\\ &\quad+[(i+2)(i+1)\{-\mu_2+i(i+1)\}-\mu_1\{i(i+1)-\mu_2\}/\{(i+3)(i+2)(i+1)-(i+3)\mu_2\}]\bar{x}^{(i+3)}, \end{aligned} \tag{14a}$$

$$u_{\bar{k}}(\bar{x})=(\bar{k}+1)[\bar{x}^{\bar{k}}-\bar{x}^{(\bar{k}+1)}]. \tag{14b}$$

Here i and $\bar{k}$ are same as defined for the clamped–guided beam. For clamped–free beam, the shape functions are as follows [26]:

$$\begin{aligned} w_i(\bar{x}) &= (i+3)(i+2)\{(i+2)(i+1)-\mu_2\}\bar{x}^{(i+1)}+[2(i+3)(i+1)\{\mu_2-i(i+2)\}\mu_1 i(i+1)/\{(i+2)(i+1)-\mu_2\}]\\ &\quad+[(i+2)(i+1)\{-\mu_2+i(i+1)\}-\mu_1 i(i+1)^2/\{(i+3)(i+2)(i+1)-(i+3)\mu_2\}\bar{x}^{(i+3)}, \end{aligned} \tag{15a}$$

$$u_k(\bar{x})=(\bar{k}+1)\bar{x}^{\bar{k}}-\bar{k}\bar{x}^{(\bar{k}+1)}. \tag{15b}$$

Here i and $\bar{k}$ are same as the previous boundary conditions.

If $[L]$ is a normalized modal matrix of $[M]^{-1}[K]$, then the linear transformation

$$\{f\}=[L]\{U\}, \tag{16}$$

transforms Eq. (11) to

$$\ddot{U}_q+(\omega_q^*)^2U_q+2\varepsilon\cos\bar{\omega}\bar{t}\sum_{p=1}^{4N}b_{qp}^*U_p=0, \quad q=1,\ldots,4N, \tag{17}$$

where $(\omega_q^*)^2$ are the distinct eigenvalues of $[M]^{-1}[K]$ and b_{qp}^* are the elements of $[B]=-[L]^{-1}[M]^{-1}[H][L]$. Also, $\varepsilon=\bar{P}_1/2<1$ for the present analysis. The complex frequency and forcing parameters in terms of real and

imaginary parts are given by

$$\omega_q^* = \omega_{q,R} + \mathrm{j}\omega_{q,I},$$
$$b_{qp}^* = b_{qp,R} + \mathrm{j}b_{qp,I}. \tag{18}$$

4. Regions of instability

The boundaries of the regions of instability for simple and combination resonances are obtained by the modified Hsu's [23] method. When the system is excited at a frequency nearly equal to twice the natural frequencies principal parametric resonance and when it is excited near a frequency, which is equal to the sum or differences of any two modal frequencies combination resonances of sum or difference types take place. Following relations are used to obtain the boundaries of the regions of instability for simple and combination resonances [27].

(1) Simple resonance case

$$|(\bar{\omega}/2) - \omega_{\alpha,R}| < \tfrac{1}{4}\chi_\alpha, \quad \alpha = 1, 2, \ldots, 4N, \tag{19}$$

where

$$\chi_\alpha = \left[\frac{4\varepsilon^2(b_{\alpha\alpha,R}^2 + b_{\alpha\alpha,I}^2)}{\omega_{\alpha,R}^2} - 16\omega_{\alpha,I}^2\right]^{1/2}. \tag{20}$$

(2) Combination resonance of sum type

$$|\bar{\omega} - (\omega_{\alpha,R} + \omega_{\beta,R})| < \chi_{\alpha\beta}, \tag{21}$$

when damping is present

$$\chi_{\alpha\beta} = \frac{(\omega_{\alpha,I} + \omega_{\beta,I})}{4(\omega_{\alpha,I}\omega_{\beta,I})^{1/2}}\left[\frac{4\varepsilon^2(b_{\alpha\beta,R}b_{\beta\alpha,R} + b_{\alpha\beta,I}b_{\beta\alpha,I})}{\omega_{\alpha,R}\omega_{\beta,R}} - 16\omega_{\alpha,I}\omega_{\beta,I}\right]^{1/2} \tag{22}$$

and for the undamped case

$$\chi_{\alpha\beta} = \varepsilon\left[\frac{b_{\alpha\beta,R}b_{\beta\alpha,R}}{\omega_{\alpha,R}\omega_{\beta,R}}\right]^{1/2}, \quad \alpha \neq \beta, \quad \alpha, \beta = 1, 2, \ldots, 4N. \tag{23}$$

(3) Combination resonance of difference type

$$|\bar{\omega} - (\omega_{\beta,R} - \omega_{\alpha,R})| < \Lambda_{\alpha\beta}, \quad \alpha > \beta, \quad \alpha, \beta = 1, 2, \ldots, 4N \tag{24}$$

when damping is present

$$\Lambda_{\alpha\beta} = \frac{(\omega_{\alpha,I} + \omega_{\beta,I})}{4(\omega_{\alpha,I}\omega_{\beta,I})^{1/2}}\left[\frac{4\varepsilon^2(b_{\alpha\beta,I}b_{\beta\alpha,I} - b_{\alpha\beta,R}b_{\beta\alpha,R})}{\omega_{\alpha,R}\omega_{\beta,R}} - 16\omega_{\alpha,I}\omega_{\beta,I}\right]^{1/2} \tag{25}$$

and for the undamped case

$$\Lambda_{\alpha\beta} = \varepsilon\left[-\frac{b_{\alpha\beta,R}b_{\beta\alpha,R}}{\omega_{\alpha,R}\omega_{\beta,R}}\right]^{1/2}. \tag{26}$$

5. Results and discussions

Here the parametric instability regions of a three-layered symmetric sandwich beam with simply supported, clamped–guided, clamped–free riveted and clamped–free boundary conditions have been determined numerically using MATLAB, version 6.0, R12. For visco-elastic materials, core loss factor (η_c) is a measure of energy dissipation capacity and the shear parameter $g = G_c/(2E_t(c/d_t)(L/d_t)^2)$ is a measure of stiffness of the material and is important in determining how much energy gets into the visco-elastic material. So these two parameters are varied in determining the instability regions for the parametrically excited beams. Also the effects of core and skin thickness on the instability regions are studied for all these boundary conditions. In the

parametric instability regions shown in the following figures, the regions enclosed by the curves are unstable and the regions outside the curves are stable. Here the ordinate $\bar{P}_1$ is the amplitude of non-dimensional dynamic load and the abscissa $\bar{\omega}$ is the non-dimensional forcing frequency. Following physical parameters are taken for the numerical analysis. The span of the beam, $L = 300\,\text{cm}$, width, $b = 50\,\text{mm}$, the top and bottom face thickness $d_t = d_b = 2\,\text{mm}$ and the core thickness, $c = 30\,\text{mm}$. The non-dimensional static load amplitude $\bar{P}_0 = 0.1$ for all the figures except for Figs. 3, 8, 13 and 18 where it is taken to be 0.5. The top and bottom faces are of steel and the core is of soft plastic foam (Divinycell H60). The mechanical properties of steel and Divinycell H60 are given in Table 1 [11]. The instability regions with different boundary conditions are discussed in the following subsections. Unless otherwise specified, the figures are plotted using higher-order theory.

5.1. Simply supported beam

Using the shape functions given in Eq. (12) the instability regions for the simply supported beam are determined and shown in Figs. 3–6 for the first three modes. Fig. 3 shows the parametric instability regions obtained using both the higher-order theory and classical theory [26] for simple resonances. One may observe that for all the three modes, the region of instability starts at a lower frequency for higher-order theory in comparison to the classical theory, which is due to the fact that, the core is considered to be more flexible in higher-order theory than in case of classical theory. Also, it is clearly observed from these figures that the instability region is wider in case of higher-order theory as compared to the classical theory. With change in $\bar{P}_0$ (say $\bar{P}_0 = 0.1$), while instability region with higher-order theory remains almost unchanged, it is observed that for lower value of $\bar{P}_1$, the instability regions with classical theory shifts towards left.

Figs. 4–6 show the influence of core loss factor (η_c) and the shear parameter (g) upon the instability region obtained by using higher-order theory. It is clearly observed that increase in core loss factor improves the stability by shifting the instability zones upwards and reducing the area of instability, which is similar to those, obtained by classical theory. It is also observed that with increase in shear parameter stability of the system improves. From the above figures it is clearly understood that to obtain a more stable system one may go for higher value of core loss factor (η_c) and shear parameter (g).

Fig. 7 shows the effect of the ratio of the core thickness to skin thickness (c/d_t) on parametric instability regions for $\eta_c = 0.1$; $g = 0.05$. It may be observed that, with increase in c/d_t, though the area of instability regions remain almost same, the instability regions move towards left, indicating that the system will become unstable at a lower frequency and forcing amplitude in all the three modes. This is due to the fact that, increase in c/d_t, will give rise to increase in mass (if c is increased) or decrease in stiffness (if d_t is decreased) of the system. In both the cases the natural frequencies of the system will decrease and hence the parametric instability region will start at a lower frequency ($\bar{\omega}$). It may be noted that, as a symmetric sandwich beam is considered in this work, variation of c/d_t and c/d_b will have the same effect.

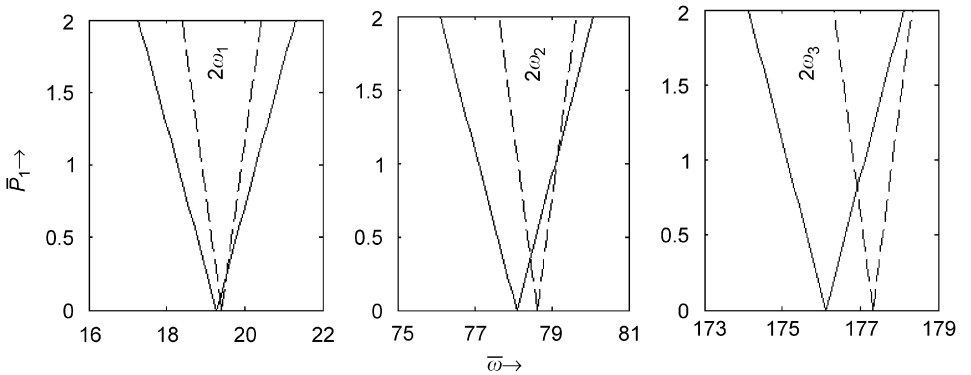

Fig. 3. Comparison of instability regions using higher-order and classical theories, $\bar{P}_0 = 0.5$, $\eta_c = 0.1$; $g = 0.05$; ——, higher-order theory; - - - - -, classical theory.

Table 1
Material properties of sandwich beam

Material	Young's modulus E (Gpa)	Shear modulus G (Gpa)	Poisson's ratio (v)	Density ρ (kg/m^3)
Steel	210	81	0.3	7900
Divinycell H60	0.056	0.022	0.27	60

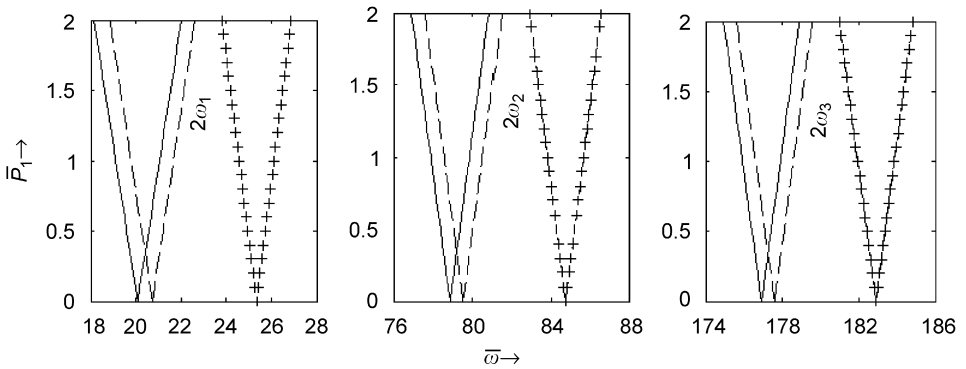

Fig. 4. Effect of shear parameter on instability regions for $\eta_c = 0.0$; ——, $g = 0.05$; - - - - -, $g = 0.1$; + + + +, $g = 0.5$.

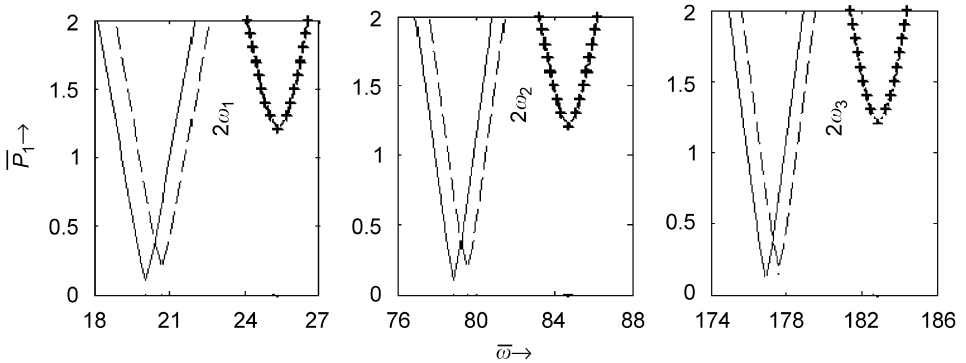

Fig. 5. Effect of shear parameter on instability regions for $\eta_c = 0.18$; ——, $g = 0.05$; - - - - -, $g = 0.1$; + + + +, $g = 0.5$.

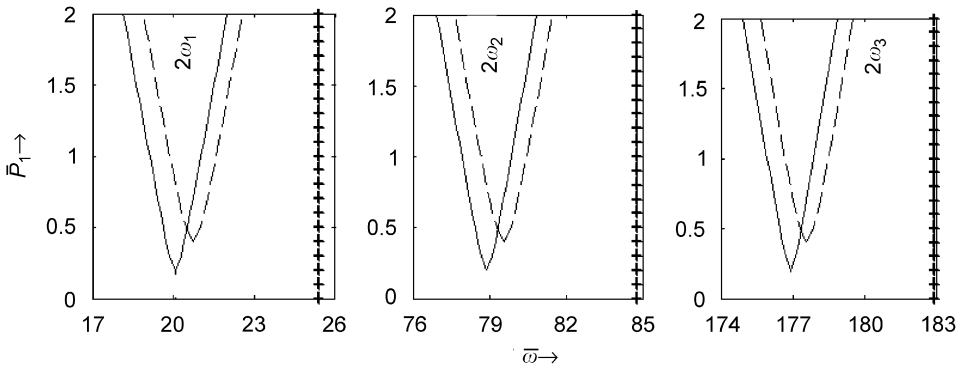

Fig. 6. Effect of shear parameter on instability regions for $\eta_c = 0.3$; ——, $g = 0.05$; - - - - -, $g = 0.1$; + + + +, $g = 0.5$.

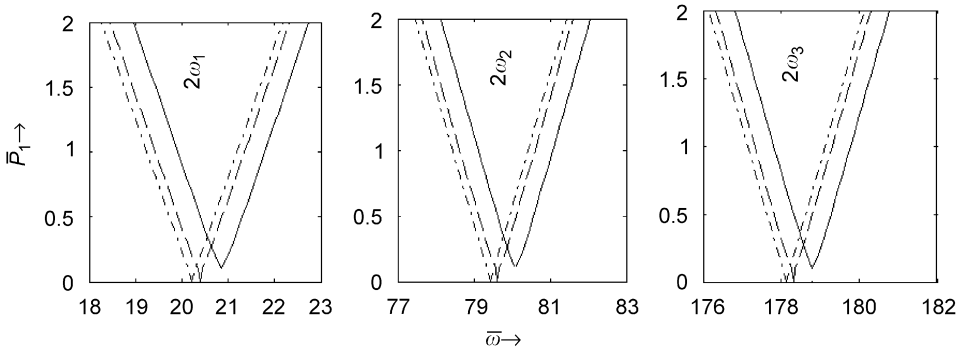

Fig. 7. Effect of the ratio of core thickness to skin thickness (c/d_t) on instability regions for $\eta_c = 0.1$, $g = 0.05$; ——, $c/d_t = 2$; - - - - -, $c/d_t = 5$; —·—·—·—·—, $c/d_t = 15$.

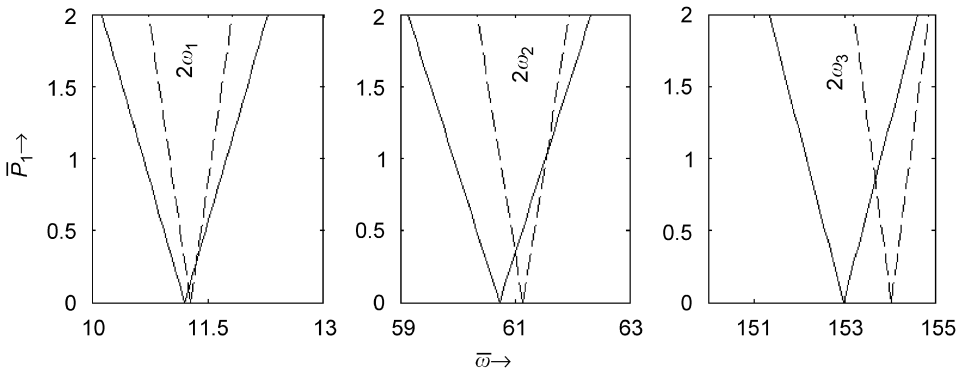

Fig. 8. Comparison of instability regions using higher-order and classical theories for $\bar{P}_0 = 0.5$, $\eta_c = 0.1$, $g = 0.05$; ——, higher-order theory; - - - - -, classical theory.

Comparing Figs. 3 and 7, it may be observed that with increase in the non-dimensional static force parameter ($\bar{P}_0$), the instability region of the system becomes wider and it starts at a lower frequency.

5.2. Clamped-guided beam

By taking same system parameters as stated before and the shape functions as given in Eq. (13), the instability regions for the clamped–guided beam are determined and shown in Figs. 8–12 for the first three modes.

In Fig. 8, the parametric instability regions obtained using both higher-order theory and classical theory [26] are compared for simple resonances. Except for higher modes and very low value of $\bar{P}_1$, it may be observed that, higher-order theory will give conservative design parameters for sandwich beam construction. The effect of core loss factor and shear parameter on instability regions are shown in Figs. 9–11. Similar to the previous case, the stability of the system improves with increase in core loss factor and shear parameter. Here the instability region is smaller than that of the previous boundary condition.

Similar to the previous boundary condition, for the same length, core-loss factor and shear parameter, with increase in c/d_t, the instability regions occur at a lower frequency and amplitude of forcing (Fig. 12). One may clearly observe from Figs. 12 and 8 that with increase in $\bar{P}_0$, parametric instability region starts at a lower frequency. This can be explained from the expression for stiffness matrix [K] (Eq. (11)), which shows that stiffness decreases with increase in $\bar{P}_0$ and hence the instability region starts at a lower frequency for higher value of $\bar{P}_0$.

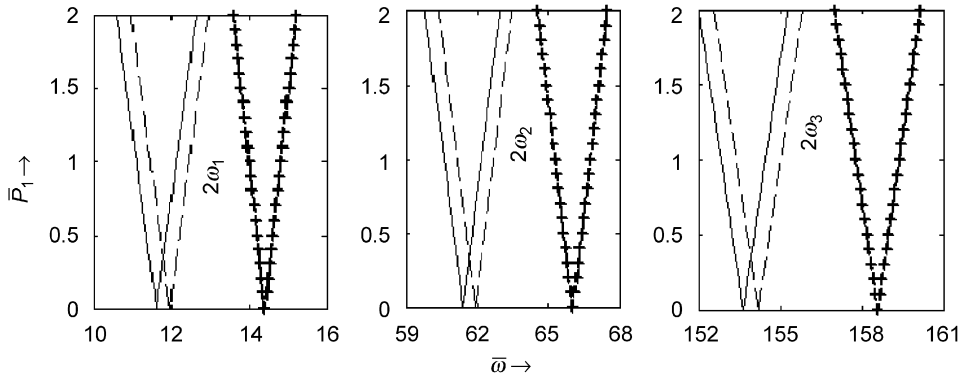

Fig. 9. Effect of shear parameter on instability regions for $\eta_c = 0$; ——, $g = 0.05$; -----, $g = 0.1$; + + + +, $g = 0.5$.

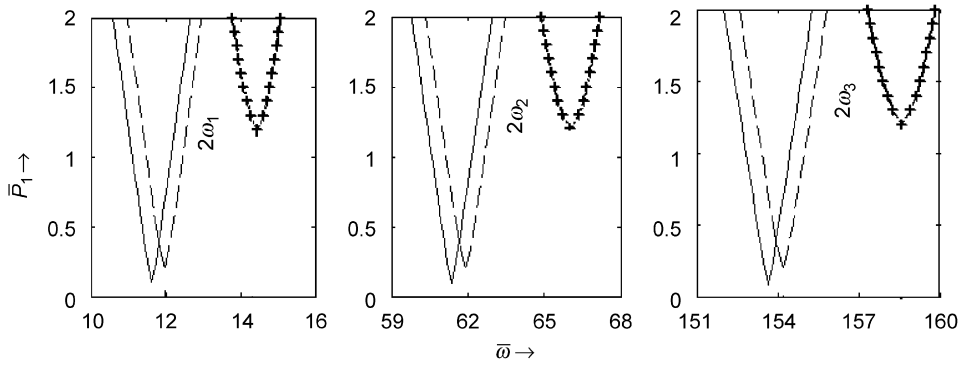

Fig. 10. Effect of shear parameter on instability regions for $\eta_c = 0.18$; ——, $g = 0.05$; -----, $g = 0.1$; + + + +, $g = 0.5$.

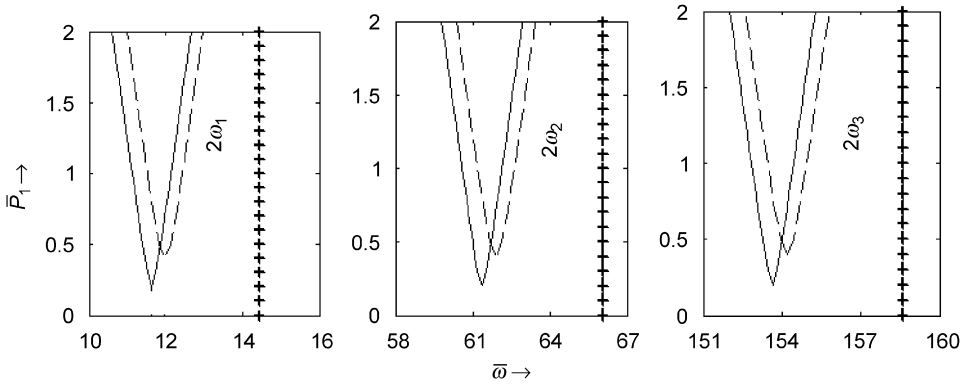

Fig. 11. Effect of shear parameter on instability regions for $\eta_c = 0.3$; ——, $g = 0.05$; -----, $g = 0.1$; + + + +, $g = 0.5$.

5.3. Clamped–free riveted beam

The instability regions for the first three modes of a clamped–free riveted beam are shown in Figs. 13–17. Here in Fig. 13, the parametric instability regions obtained by both the higher-order theory and classical theory [26] are compared.

It may be observed that by analyzing a soft-cored sandwich beam by classical theory will yield erroneous result as the actual system response may be unstable, e.g., point A on Fig. 13, is stable considering classical theory, but unstable considering higher-order theory. But in third mode, point B is stable considering higher-order theory, but unstable considering classical theory. Hence, except for higher modes and for very low forcing amplitude, one may obtain a safer design by considering higher-order theory.

Here, the non-dimensional forcing frequency at which the instability region starts is less than those obtained by considering the previous two boundary conditions. Also it may be observed that the instability region in this case is more than those for the simply supported and clamped–guided cases.

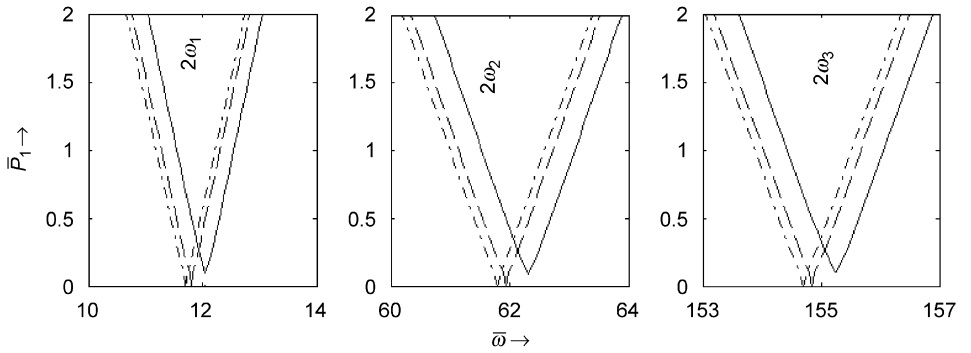

Fig. 12. Effect of the ratio of core thickness to skin thickness (c/d_t) on instability regions for $\eta_c = 0.1$, $g = 0.05$; ——, $c/d_t = 2$; – – – –, $c/d_t = 5$; – · – · – · – ·, $c/d_t = 15$.

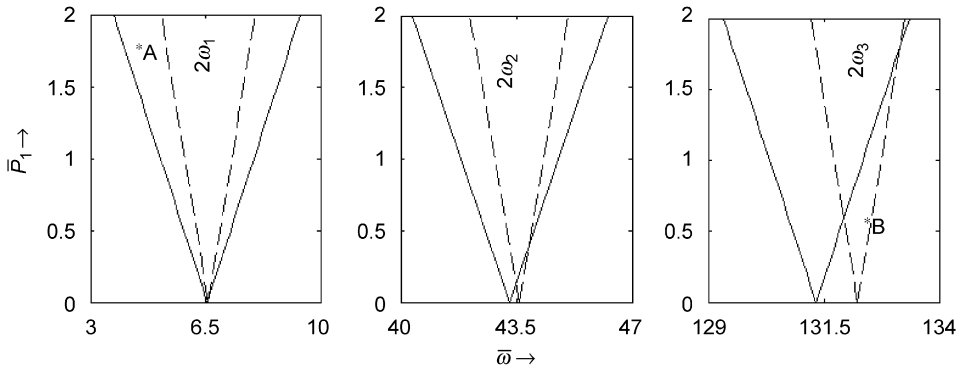

Fig. 13. Comparison of instability regions using higher-order and classical theories for $\tilde{P}_0 = 0.5$, $\eta_c = 0.1$, $g = 0.05$; ——, higher-order theory; - - - - -, classical theory.

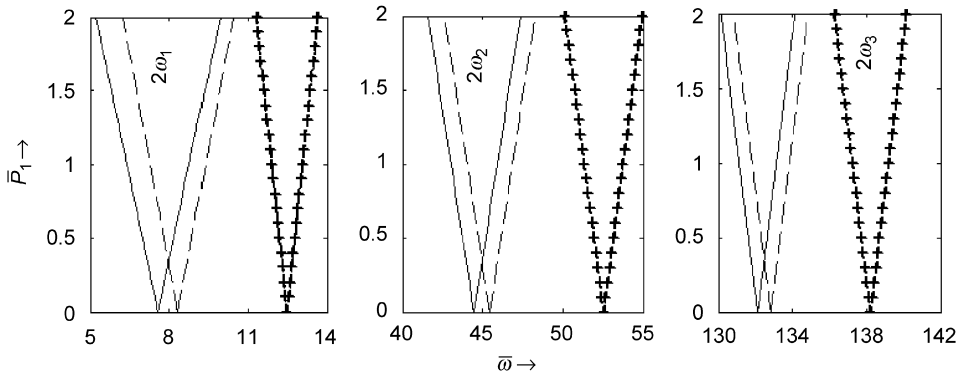

Fig. 14. Effect of shear parameter on instability regions for $\eta_c = 0$; ——, $g = 0.05$; - - - - -, $g = 0.1$; + + + +, $g = 0.5$.

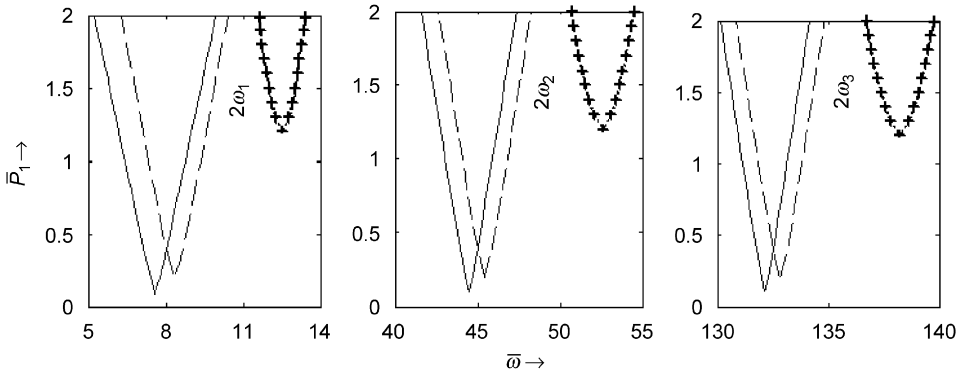

Fig. 15. Effect of shear parameter on instability regions for $\eta_c = 0.18$; ——, $g = 0.05$; - - - - -, $g = 0.1$; + + + +, $g = 0.5$.

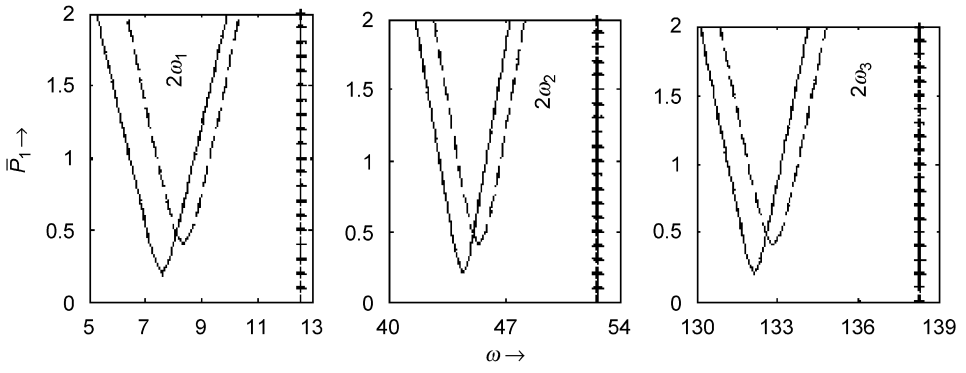

Fig. 16. Effect of shear parameter on instability regions for $\eta_c = 0.3$; ——, $g = 0.05$; - - - - -, $g = 0.1$; + + + +, $g = 0.5$.

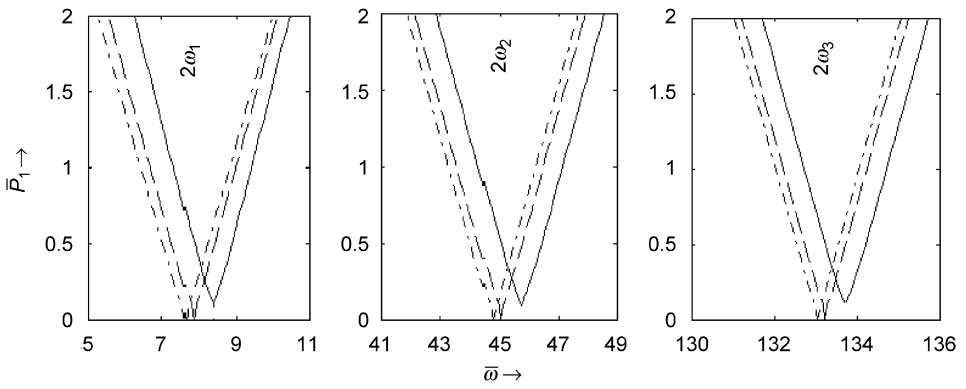

Fig. 17. Effect of the ratio of core thickness to skin thickness (c/d_t) on instability regions for $\eta_c = 0.1$, $g = 0.05$; ——, $c/d_t = 2$; – – – –, $c/d_t = 5$; – · – · – · – ·, $c/d_t = 15$.

Figs. 14–16 show the influence of core loss factor (η_c) and the shear parameter (g) upon the instability region and one may note that for the same η_c and g, the stability region in this case is more improved than the previous two boundary conditions.

Similar to the previous two cases, in this case also increase in c/d_t ratio (Fig. 17) moves the instability regions towards left. Further, due to this clamped–free riveted boundary condition, the instability regions occur at a

lower frequency in comparison to the previous two cases. From Figs. 13 and 17, one may observe the shifting of the parametric instability region towards right with increase in the static force amplitude.

5.4. Clamped–free beam

Using the shape functions (Eq. (15)) for the clamped–free beam, the instability regions for the first three modes are determined and shown in Figs. 18–22.

Using higher-order theory and classical theory the parametric instability regions for simple resonances are shown in Fig. 18. Here also, higher-order theory gives a conservative design for lower modes. In this case, the non-dimensional forcing frequency at which the instability region starts is the lowest among all the boundary conditions, which are discussed here. It may also be observed that the instability region for this case is more in comparison to simply supported and clamped-guided boundary conditions. The variation in instability regions for clamped–free riveted and this case is almost negligible.

Figs. 19–21 show the influence of core loss factor (η_c) and the shear parameter (g) upon the instability region and it is observed that with increase in core loss factor and shear parameter stability of the system improves.

Fig. 22 shows the parametric instability regions for a cantilevered sandwich beam for different values of c/d_t ratio and one may obtain similar observations as in the previous boundary conditions.

For all the boundary conditions the system is always found to be stable at combination resonances of sum and difference type. In these cases, for simple resonances it is observed that with increase in shear parameter the instability plot moves upward implying that there exists critical forcing amplitude below which the system

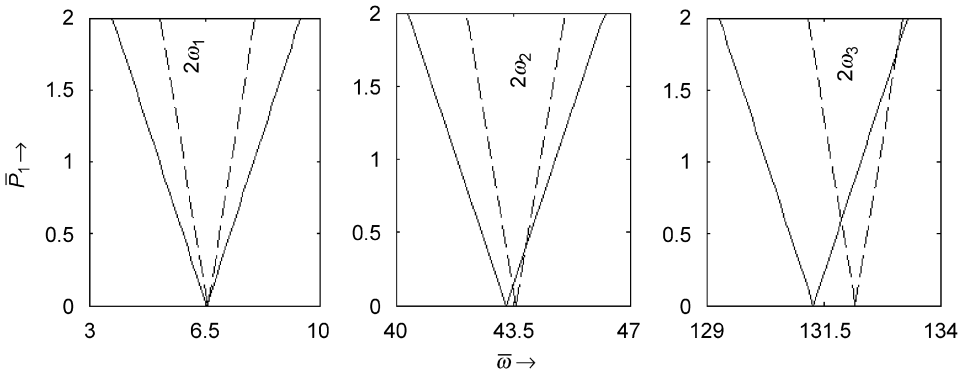

Fig. 18. Comparison of instability regions using higher-order and classical theories for $\bar{P}_0 = 0.5$, $\eta_c = 0.1$, $g = 0.05$; ——, higher-order theory; - - - - -, classical theory.

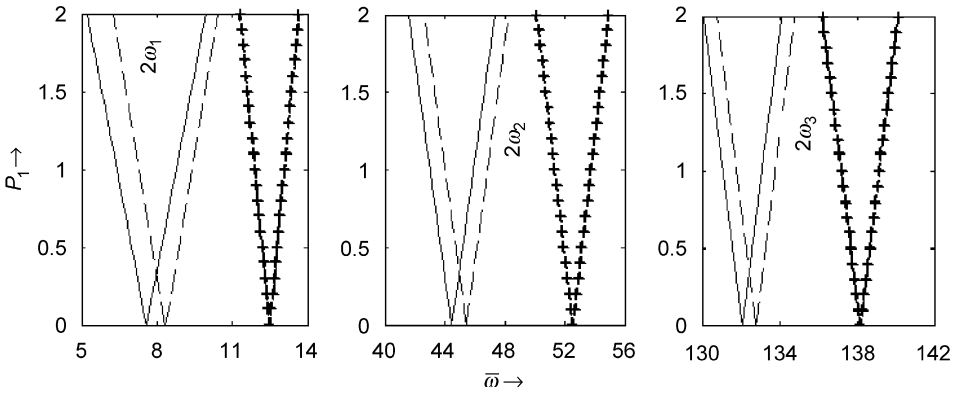

Fig. 19. Effect of shear parameter on instability regions for $\eta_c = 0$; ——, $g = 0.05$; - - - - -, $g = 0.1$; + + + +, $g = 0.5$.

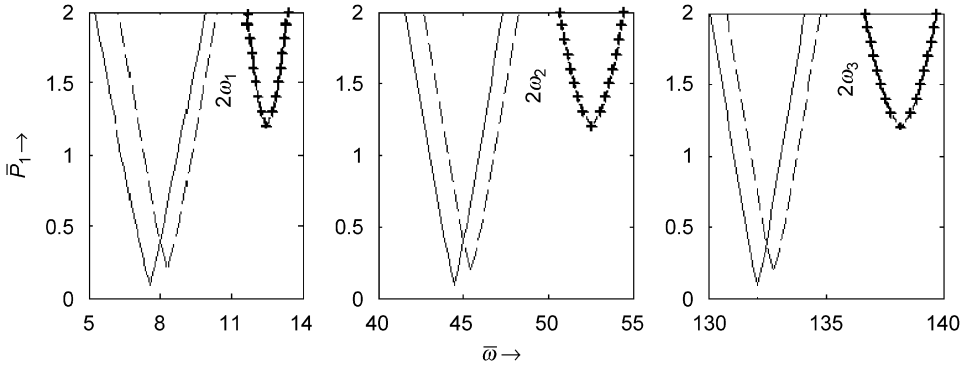

Fig. 20. Effect of shear parameter on instability regions for $\eta_c = 0.18$; ——, $g = 0.05$; - - - - -, $g = 0.1$; + + + +, $g = 0.5$.

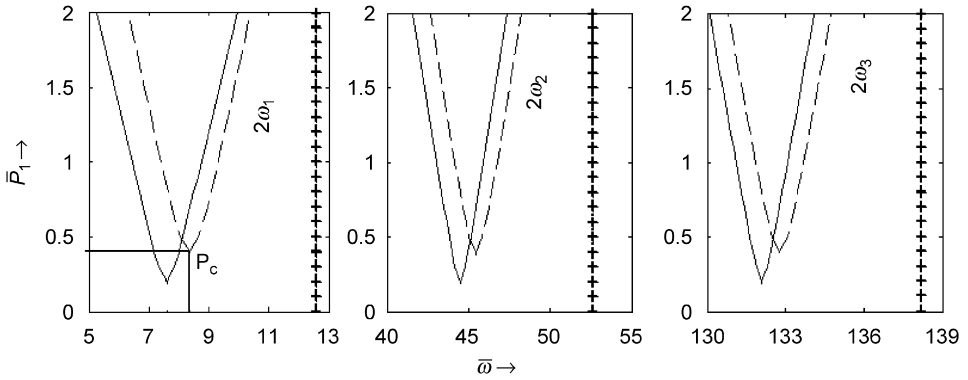

Fig. 21. Effect of shear parameter on instability regions for $\eta_c = 0.3$; ——, $g = 0.05$; - - - - -, $g = 0.1$; + + + +, $g = 0.5$.

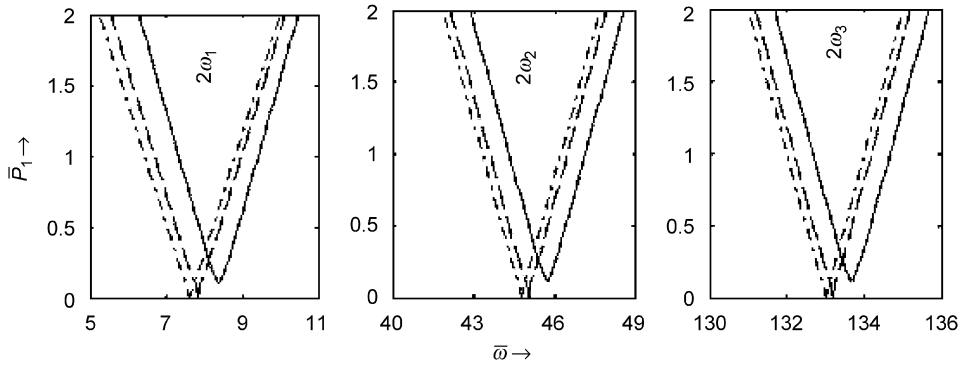

Fig. 22. Effect of the ratio of core thickness to skin thickness (c/d_t) on instability regions for $\eta_c = 0.1$, $g = 0.05$; ——, $c/d_t = 2$; – – – –, $c/d_t = 5$; –·–·–·–·–, $c/d_t = 15$.

is always stable. For example, when a cantilevered sandwich beam with $\eta_c = 0.3$ and $g = 0.1$ is excited near twice the first natural frequency $\bar{\omega} = 8.2$; the system will not vibrate if the forcing amplitude is less than 0.485 (point P_c on Fig. 21). But for the same η_c and $g = 0.05$, with same amplitude of forcing, the system will vibrate at a slightly less frequency (say $\bar{\omega} = 7.8$). Again with increase in shear parameter, the instability region shifts towards right and hence, for same forcing amplitude, the system becomes unstable at a higher frequency. As the shear parameter $g = G_c/(2E_t(c/d_t)(L/d_t)^2)$, is a function of dimension and material properties of both skin and core material, using the above stability charts, a designer will be able to construct sandwich beams having very less or vibration free structures.

6. Conclusions

The analysis for finding the parametric instability regions of a three-layered, symmetric sandwich beam with soft viscoelastic core, subjected to periodic axial end load is presented using higher-order theory. The results of the classical theory are also determined for comparison purpose. In this work, the parametric instability regions with simple and combination resonances for simply supported, clamped–guided, clamped–free riveted and clamped–free end conditions are investigated. In all these cases, the modal frequencies obtained by using higher-order theory are found to be lower than those obtained by using classical theory. Also, wide instability regions are observed using the higher-order theory in comparison to those obtained by classical theory. It is noticed that use of classical theory for soft-cored sandwich beam will give erroneous result and except at very low amplitude of forcing and higher modes, one will obtain a very safe design using higher-order theory. Hence, it is recommended to use higher-order theory for soft-cored sandwich beam to find the instability regions.

For all the considered boundary conditions, it is observed that by increasing the core loss factor (η_c) and/or shear parameter (g) improve the stability of the system as the instability region moves upwards and shifts towards right. For the same length, core-loss factor and shear parameter, with increase in the ratio of core thickness to skin thickness, the instability regions occur at a lower frequency and amplitude of forcing. Also it is observed that with decrease in static amplitude of forcing $\bar{P}_0$, the instability region starts at a higher frequency. The effect of c/d_t on the parametric instability regions is also studied for all the boundary conditions and it is observed that lower value of c/d_t improves the stability of the system. In all the cases instability charts are plotted for a wide range of system parameters.

By using the parametric instability region charts, it will be easier for the designer to choose dimension, material of the sandwich beam and the operating frequency and amplitude of forcing parameters to avoid unnecessary vibration of the system. This analysis is general and can be applied to sandwich beams with any type of construction and a flexible core.

Appendix

$$(M_{11})_{ij} = (\bar{m}_t + m_c/3)\left(\int_0^1 w_i w_j \,\mathrm{d}\bar{x}\right) + \{(\bar{m}_c/12)(d_t/L)^2\}\left(\int_0^1 w_i' w_j' \,\mathrm{d}\bar{x}\right) + \{(\bar{m}_c/576)(d_t/c)(1+d_t/c)\big(c/L\big)^4(\xi_c/\phi_c)\}\left(\int_0^1 w_i'' w_j'' \,\mathrm{d}\bar{x}\right),$$

$$(M_{12})_{ij} = (\bar{m}_c/6)\left(\int_0^1 w_i w_j \,\mathrm{d}\bar{x}\right) - \{(\bar{m}_c/24)(d_t d_b/L^2)\}\left(\int_0^1 w_i' w_j' \,\mathrm{d}\bar{x}\right) + \{(\bar{m}_c/576)(d_b/c)(1+d_t/c)(c/L)^4(\xi_c/\phi_c)\}\left(\int_0^1 w_i'' w_j'' \,\mathrm{d}\bar{x}\right),$$

$$(M_{13})_{ij} = -\{(\bar{m}_t + \bar{m}_c/6)(1/48)(1+d_t/c)(c/L)^3(\xi_c/\phi_c)\} \times \left(\int_0^1 w_u'' u_j' \,\mathrm{d}\bar{x}\right) - \{(m_c/6)(d_t/L)\}\left(\int_0^1 w_i' u_j \,\mathrm{d}\bar{x}\right),$$

$$(M_{14})_{ij} = \{(1/48)(\bar{m}_b + \bar{m}_c/6)(1+d_t/c)(c/L)^3(\xi_c/\phi_c)\} \times \left(\int_0^1 w_i'' u_j'' \,\mathrm{d}\bar{x}\right) - \{(\bar{m}_c/12)(d_t/L)\}\left(\int_0^1 w_i' u_j \,\mathrm{d}\bar{x}\right),$$

$$(M_{21})_{ij} = (\bar{m}_c/6)\left(\int_0^1 w_i w_j \,\mathrm{d}\bar{x}\right) - \{(\bar{m}_c/24)(d_t d_b/L^2)\}\left(\int_0^1 w_i' w_j' \,\mathrm{d}\bar{x}\right) + \{(\bar{m}_c/576)(d_t/c)(1+d_b/c)(c/L)^4(\xi_c/\phi_c)\}\left(\int_0^1 w_i'' w_j'' \,\mathrm{d}\bar{x}\right),$$

$$(M_{22})_{ij} = (\bar{m}_b + \bar{m}_c/3)\left(\int_0^1 w_i w_j \,\mathrm{d}\bar{x}\right) - \{(\bar{m}_c/12)(d_t/L)^2\}\int_0^1 w_i' w_j' \,\mathrm{d}\bar{x} + \{(\bar{m}_c/576)(d_b/c)(1+d_b/c)(c/L)^4(\xi_c/\phi_c)\}\left(\int_0^1 w_i'' w_j'' \,\mathrm{d}\bar{x}\right),$$

$$(M_{23})_{ij} = -\{(1/48(\bar{m}_t + \bar{m}_c/6)(1+d_b/c)(c/L)^3(\xi_c/\phi_c)\} \times\left(\int_0^1 w_i'' u_j' \,\mathrm{d}\bar{x}\right) + \{(\bar{m}_c/12)(d_b/L)\}\left(\int_0^1 w_i' u_j \,\mathrm{d}\bar{x}\right),$$

$$(M_{24})_{ij} = \{(1/48)(\bar{m}_b + \bar{m}_c/6)(1+d_b/c)(c/L)^3(\xi_c/\phi_c)\} \times\left(\int_0^1 w_i'' u_j' \,\mathrm{d}\bar{x}\right) + (\bar{m}_c/6)(d_b/L)\left(\int_0^1 w_i' u_j \,\mathrm{d}\bar{x}\right),$$

$$(M_{31})_{ij} = -\{(\bar{m}_c/288)(d_t/c)(c/L)^3(\xi_c/\phi_c)\}\left(\int_0^1 u_i'' w_j' \,\mathrm{d}\bar{x}\right) - \{(\bar{m}_c/6)(d_t/L)\}\left(\int_0^1 u_i' w_j \,\mathrm{d}\bar{x}\right),$$

$$(M_{32})_{ij} = \{(\bar{m}_c/12)(d_b/L)\}\left(\int_0^1 u_i' w_j \,\mathrm{d}\bar{x}\right) - \{(\bar{m}_c/288)(d_b/c)(c/L)^3(\xi_c/\phi_c)\}\left(\int_0^1 u_i'' w_j' \,\mathrm{d}\bar{x}\right),$$

$$(M_{33})_{ij} = -\{(1/24)(\bar{m}_t + \bar{m}_c/6)(c/L)^2(\xi_c/\phi_c)\}\left(\int_0^1 u_i' u_j' \,\mathrm{d}\bar{x}\right) - (\bar{m}_t + \bar{m}_c/3)\left(\int_0^1 u_i u_j \,\mathrm{d}\bar{x}\right),$$

$$(M_{34})_{ij} = \{(-\bar{m}_c/6)\}\left(\int_0^1 u_i u_j \,\mathrm{d}\bar{x}\right) + \{(1/24)(\bar{m}_b + \bar{m}_c/6)(c/L)^2(\xi_c/\phi_c)\}\left(\int_0^1 u_i' u_j' \,\mathrm{d}\bar{x}\right),$$

$$(M_{41})_{ij} = -\{(\bar{m}_c/12)(d_t/L)\}\left(\int_0^1 u_i' w_j \,\mathrm{d}\bar{x}\right) + \{(\bar{m}_c/288)(d_t/c)(c/L)^3(\xi_c/\phi_c)\}\left(\int_0^1 u_i'' w_j' \,\mathrm{d}\bar{x}\right),$$

$$(M_{42})_{ij} = \{(\bar{m}_c/6)(d_b/L)\}\left(\int_0^1 u_i' w_j \,\mathrm{d}\bar{x}\right) + \{(\bar{m}_c/288)(d_b/c)(c/L)^3(\xi_c/\phi_c)\}\left(\int_0^1 u_i'' w_j' \,\mathrm{d}\bar{x}\right),$$

$$(M_{43})_{ij} = \{(-\bar{m}_c/6)\}\left(\int_0^1 u_i u_j \,\mathrm{d}\bar{x}\right) + \{(1/24)(\bar{m}_t + \bar{m}_c/6)(c/L)^2(\xi_c/\phi_c)\}\left(\int_0^1 u_i' u_j' \,\mathrm{d}\bar{x}\right),$$

$$(M_{44})_{ij} = -\{(\bar{m}_b + \bar{m}_c/3)\}\left(\int_0^1 u_i u_j \,\mathrm{d}\bar{x}\right) - \{(1/24)(\bar{m}_b + \bar{m}_c/6)(c/L)^2(\xi_c/\phi_c)\}\left(\int_0^1 u_i' u_j' \,\mathrm{d}\bar{x}\right),$$

$$(K_{11})_{ij} = \left\{(1/4)(1+d_t/c)^2\xi_c\right\}\left(\int_0^1 w_i' w_j' \mathrm{d}\bar{x}\right) + \{(1/12)(d_t/L)^2\phi_t\}\left(\int_0^1 w_i'' w_j'' \,\mathrm{d}\bar{x}\right) + \{\phi_c(L/c)^2\}\left(\int_0^1 w_i w_j \,\mathrm{d}\bar{x}\right),$$

$$(K_{12})_{ij} = -\{\phi_c(L/c)^2\}\left(\int_0^1 w_i w_j \,\mathrm{d}\bar{x}\right) + \{(1/4)(1+d_t/c)(1+d_b/c)\xi_c\}\left(\int_0^1 w_i' w_j' \,\mathrm{d}\bar{x}\right),$$

$$(K_{13})_{ij} = -\{(1/2)(L/c)(1+d_t/c)\xi_c\}\left(\int_0^1 w_i' u_j \,\mathrm{d}\bar{x}\right) - \{(1/48)(c/L)^3(1+d_t/c)(\xi_c/\phi_c)\phi_t\}\left(\int_0^1 w_u''' u_j'' \,\mathrm{d}\bar{x}\right),$$

$$(K_{14})_{ij} = \{(1/2)(L/c)(1+d_t/c)\xi_c\}\left(\int_0^1 w_i' u_j \,\mathrm{d}\bar{x}\right) + \{(1/48)(c/L)^3(1+d_t/c)(\xi_c/\phi_c)\phi_b\}\left(\int_0^1 w_i''' u_j'' \,\mathrm{d}\bar{x}\right),$$

$$(K_{21})_{ij} = -\{\phi_c(L/c)^2\}\left(\int_0^1 w_i w_j \,\mathrm{d}\bar{x}\right) + \{(1/4)(1+d_t/c)(1+d_b/c)\xi_c\}\left(\int_0^1 w_i' w_j' \,\mathrm{d}\bar{x}\right),$$

$$(K_{22})_{ij} = \{(1/4)(1+d_b/c)^2\xi_c\}\left(\int_0^1 w_i' w_j' \,\mathrm{d}\bar{x}\right) + \{(1/12)(d_b/L)^2\phi_b\}\left(\int_0^1 w_i'' w_j'' \,\mathrm{d}\bar{x}\right) + \{\phi_c(L/c)^2\}\left(\int_0^1 w_i w_j \mathrm{d}\bar{x}\right),$$

$$(K_{23})_{ij} = \{(-1/2)(L/c)(1+d_b/c)\xi_c\}\left(\int_0^1 w_i' u_j \,\mathrm{d}\bar{x}\right) - \{(1/48)(c/L)^3(1+d_b/c)(\xi_c/\phi_c)\phi_t\}\left(\int_0^1 w_i''' u_j'' \,\mathrm{d}\bar{x}\right),$$

$$(K_{24})_{ij} = \{(1/2)(L/c)(1+d_b/c)\xi_c\}\left(\int_0^1 w_i' u_j \,\mathrm{d}\bar{x}\right) + \{(1/48)(c/L)^3(1+d_b/c)(\xi_c/\phi_c)\phi_b\}\left(\int_0^1 w_i''' u_j'' \,\mathrm{d}\bar{x}\right),$$

$$(K_{31})_{ij} = \{(-1/2)(L/c)(1+d_t/c)\xi_c\}\left(\int_0^1 u_i' w_j \,\mathrm{d}\bar{x}\right),$$

$$(K_{32})_{ij} = \{(-1/2)(L/c)(1+d_b/c)\xi_c\}\left(\int_0^1 u_i' w_j \,\mathrm{d}\bar{x}\right),$$

$$(K_{33})_{ij} = (-\phi_t)\left(\int_0^1 u_i' u_j' \,\mathrm{d}\bar{x}\right) - \{(L/c)^2\xi_c\}\left(\int_0^1 u_i u_j \mathrm{d}\bar{x}\right) - \{(1/24)(c/L)^2(\xi_c/\phi_c)\phi_t\}\left(\int_0^1 u_i'' u_j'' \,\mathrm{d}\bar{x}\right),$$

$$(K_{34})_{ij} = \{(L/c)^2\xi_c\}\left(\int_0^1 u_i u_j \,\mathrm{d}\bar{x}\right) + \{(1/24)(c/L)^2(\xi_c/\phi_c)\phi_b\}\left(\int_0^1 u_i'' u_j'' \,\mathrm{d}\bar{x}\right),$$

$$(K_{41})_{ij} = \{(1/2)(L/c)(1+d_t/c)\xi_c\}\left(\int_0^1 u_i' w_j \,\mathrm{d}\bar{x}\right),$$

$$(K_{42})_{ij} = \{(1/2)(L/c)(1+d_b/c)\xi_c\}\left(\int_0^1 u_i' w_j \,\mathrm{d}\bar{x}\right),$$

$$(K_{43})_{ij} = \{(L/c)^2\xi_c\}\left(\int_0^1 u_i u_j \,\mathrm{d}\bar{x}\right) + \{(1/24)(c/L)^2(\xi_c/\phi_c)\phi_t\}\left(\int_0^1 u_i'' u_j'' \,\mathrm{d}\bar{x}\right),$$

$$(K_{44})_{ij} = (-\phi_b)\left(\int_0^1 u_i' u_j' \,\mathrm{d}\bar{x}\right) - \{(L/c)^2\xi_c\}\left(\int_0^1 u_i u_j \mathrm{d}\bar{x}\right) - \{(1/24)(c/L)^2(\xi_c/\phi_c)\phi_b\}\left(\int_0^1 u_i'' u_j'' \,\mathrm{d}\bar{x}\right),$$

$$(H)_{11} = \int_0^1 w_i' w_j' \,\mathrm{d}\bar{x},$$

$$(H)_{22} = \int_0^1 w_i' w_j' \,\mathrm{d}\bar{x},$$

In the above relations, $(\,)' = \partial(\,)/\partial\bar{x}$, and the sub-matrices, which are not covered by the above elements, should be treated as null.

References

[1] R.A. Ditaranto, Theory of vibratory bending for elastic and viscoelastic layered finite-length beams, *Journal of Applied Mechanics* 32 (1965) 881–886.

[2] N.T. Asnani, B.C. Nakra, Vibration analysis of multilayered beams with alternate elastic and viscoelastic layers, *Journal of Institution of Engineers (India)—Mechanical Engineering Division* 50 (1970) 187–193.

[3] D.J. Mead, Loss factors and resonant frequencies of periodic damped sandwich plates, *Journal of Engineering for Industry* 98 (1976) 75–80.

[4] M.J. Yan, E.H. Dowell, Governing equations for vibrating constrained-layer damping sandwich plates and beams, *Journal of Applied Mechanics* 39 (1972) 1041–1046.

[5] A. Bhimaraddi, Sandwich beam theory and the analysis of constrained layer damping, *Journal of Sound and Vibration* 179 (4) (1995) 591–602.

[6] M.A. Trindade, A. Benjeddou, R. Ohayon, Parametric analysis of the vibration control of sandwich beams through shear-based piezoelectric actuation, *Journal of Intelligent Material Systems and Structures* 10 (5) (1999) 377–385.

[7] B.C. Nakra, Structural dynamic modification using additive damping, *Sadhana* 25 (3) (2000) 277–289.

[8] Y. Frostig, M. Baruch, Bending of sandwich beams with transversely flexible core, *American Institute of Aeronautics and Astronautics Journal* 27 (1990) 523–531.

[9] Y. Frostig, M. Baruch, Free vibrations of sandwich beams with a transversely flexible core: a higher order approach, *Journal of Sound and Vibration* 176 (2) (1994) 195–208.

[10] Y. Frostig, Buckling of sandwich panels with flexible core-high order theory, *International Journal of Solids and Structures* 35 (3–4) (1998) 183–204.

[11] H.F. Bremen, V.S. Sokolinsky, J.A. Lavoie, S.R. Nutt, Experimental and analytical study of natural vibration modes of soft-core sandwich beams, *Proceedings of the 46th International SAMPE Symposium and Exhibition*, held in Long Beach, CA, May 6–10, 2001.

[12] V.S. Sokolinsky, H.F. Bremen, J.A. Lavoie, S.R. Nutt, Analytical and experimental study of free vibration response of soft-core sandwich beams, *Journal of Sandwich Structures and Materials* 6 (3) (2004) 239–261.

[13] V.S. Sokolinsky, S.R. Nutt, Consistent higher-order dynamic equations for soft-core sandwich beams, *AIAA Journal* 42 (2) (2004) 374–382.

[14] Y. Frostig, O.T. Thomsen, High-order free vibration of sandwich panels with a flexible core, *International Journal of Solids and Structures* 41 (2004) 1697–1724.

[15] M. Yang, P. Qiao, Higher-order impact modeling of sandwich structures with flexible core, *International Journal of Solids and Structures* 42 (20) (2005) 5460–5490.

[16] Q. Liu, Y. Zhao, Natural frequency analysis of a sandwich panel with soft core based on a refined shear deformation model, *Composite Structures* 72 (2006) 364–374.

[17] A.K. Noor, W.S. Burton, C.W. Bert, Computational models for sandwich panels and shells, *Applied Mechanics Review, ASME* 49 (3) (1996) 155–188.

[18] C.T. Sun, Y.P. Lu, *Vibration Damping of Structural Elements*, Prentice-Hall, Englewood Cliffs, NJ, 1995.

[19] I.G.J. David, *Handbook of Viscoelastic Vibration Damping*, Wiley, England, 2001.

[20] A.H. Nayfeh, D.T. Mook, *Non-linear Oscillations*, Wiley Interscience, New York, 1979.

[21] M.P. Cartmell, *Introduction to Linear Parametric and Non-linear Vibrations*, Chapman & Hall, London, 1990.

[22] N.R. Bauld Jr., Dynamic stability of sandwich columns under pulsating axial loads, *AIAA Journal* 5 (1967) 1514–1516.

[23] H. Saito, K. Otomi, Parametric response of viscoelastically supported beams, *Journal of Sound and Vibration* 63 (1979) 169–178.

[24] S. Chonan, Vibration and stability of sandwich beams with elastic bonding, *Journal of Sound and Vibration* 85 (4) (1982) 525–537.

[25] R.C. Kar, T. Sujata, Dynamic stability of a tapered symmetric sandwich beam, *Computers & Structures* 40 (1991) 1441–1449.

[26] K. Ray, R.C. Kar, Parametric instability of a sandwich beam with various boundary conditions, *Computers & Structures* 55 (1995) 857–870.

[27] K. Ray, R.C. Kar, Parametric instability of multi-layered sandwich beams, *Journal of Sound and Vibration* 193 (3) (1996) 631–644.

[28] C.S. Hsu, On the parametric excitation of a dynamic system having multiple degrees of freedom, *Journal of Applied Mechanics, ASME* 30 (1963) 367–372.